Eur. Phys. J. B **49**, 157–165 (2006)
DOI: 10.1140/epjb/e2006-00037-9

THE EUROPEAN PHYSICAL JOURNAL B

Time-resolved nuclear spin-dependent small-angle neutron scattering from polarised proton domains in deuterated solutions

B. van den Brandt[1], H. Glättli[2], I. Grillo[3], P. Hautle[1], H. Jouve[4], J. Kohlbrecher[1], J.A. Konter[1], E. Leymarie[2], S. Mango[1] , R.P. May[3], A. Michels[1,a], H.B. Stuhrmann[4,5], and O. Zimmer[6]

[1] Paul Scherrer Institute, 5232 Villigen PSI, Switzerland
[2] Commissariat à l'Énergie Atomique, CEA Saclay, DSM/DRECAM/SPEC, 91191 Gif-sur-Yvette Cedex, France
[3] Institut Laue Langevin, 38042 Grenoble Cedex 9, France
[4] Institut de Biologie Structurale Jean-Pierre Ebel, CEA/CNRS/UJF, 38027 Grenoble Cedex 1, France
[5] GKSS Forschungszentrum, 21502 Geesthacht, Germany
[6] Technische Universität München, James-Franck-Strasse, 85748 Garching, Germany

Received 29 March 2005 / Received in final form 6 November 2005
Published online 17 February 2006 –

Abstract. We have investigated the process of dynamic proton polarisation by means of time-resolved polarised small-angle neutron scattering (SANS) on frozen solutions of EHBA-Cr^V molecules in glycerol-water mixtures as a function of the concentration of EHBA-Cr^V and for different degrees of deuteration of the solvent. In the EHBA-Cr^V complex, the spins of the 20 protons which surround the paramagnetic Cr^V can be oriented using the method of dynamic nuclear polarisation (DNP), thereby offering the possibility to create locally a nuclear spin-dependent contrast for SANS. The time constants which describe the build-up of polarisation around the paramagnetic centre and the subsequent diffusion of polarisation in the solvent were determined by analysing the temporal evolution of the nuclear polarisation, which in turn was obtained by fitting a core-shell model to the time-dependent SANS curves. The results on the spin dynamics obtained using the scattering function of a core-shell could be independently confirmed by evaluating the integrated SANS intensity. A thermodynamic one-centre model is presented which is able to reproduce the observed dependence of the proton polarisation times on the proton concentration of the solvent.

PACS. 61.12.Ex Neutron scattering (including small-angle scattering) – 76.70.Fz Double nuclear magnetic resonance (DNMR), dynamical nuclear polarisation

1 Introduction

The method of dynamic nuclear polarisation (DNP) [1–3] provides a powerful tool for the alteration of the neutron scattering from nuclei possessing a non-zero nuclear spin. A necessary prerequisite for DNP is the existence of unpaired electrons in the sample. On irradiation with microwaves of frequency close to the electron paramagnetic resonance frequency, the polarisation of the electron spin system, which at typical experimental DNP conditions of $T = 1\,\mathrm{K}$ and $B \geq 2.5\,\mathrm{T}$ is close to unity, can be transferred to the nearby nuclei, taking advantage of the dipolar interaction between the electrons and the nuclear spins. For samples containing protons with nuclear spin $\frac{1}{2}$ — the most important nucleus for neutron scattering studies in soft matter — the change of the nuclear polarisation induced by DNP, relative to the thermal equilibrium polarisation which is given by Boltzmann statistics, is typically two orders of magnitude. Since the scattering length of the proton depends on the orientation of its spin relative to the orientation of the spin of the incident neutron [4], and since (by appropriate choice of the irradiating microwave frequency) DNP allows one to polarise the protons either positively or negatively, the ensuing coherent and incoherent scattering cross section can be varied significantly.

However, due to the rather complex experimental requirements (low temperatures, high magnetic fields, microwaves and NMR for DNP, incident polarised neutron beam, etc.) only a few experiments which combine neutron scattering with DNP have been reported to date (see, e.g., Refs. [5–20] and references therein). Nuclear spin-dependent neutron scattering has already been reported by Shull and Ferrier [21] in a single crystal of vanadium, polarised by "brute-force". Hayter, Jenkin, and White [7] combined DNP with neutron scattering. These

[a] *Present address:* FR 7.3 Technische Physik, Universität des Saarlandes, Postfach 151150, Geb. D2 2, 66041 Saarbrücken, Germany.
e-mail: andreas.michels@mx.uni-saarland.de

authors measured the spin-dependent Bragg diffraction from dynamically-polarised protons in a single crystal of lanthanum magnesium nitrate, $La_2Mg_3(NO_3)_{12} \cdot 24\,H_2O$, doped with 1 % of $^{142}Nd^{3+}$. It was already recognised then [7] that combining DNP with neutron scattering offers the unique possibility to label certain spin sites in complex crystals by a suitable paramagnetic centre. Later, small-angle neutron scattering (SANS) using polarised [10,12,14–16] and unpolarised neutrons [11] has been utilised to probe nuclear-polarisation-enhanced scattering on larger objects such as for example the macromolecule bovine serum albumin in a deuterated matrix [12]. It must be emphasised however that in almost all of the above mentioned SANS studies "steady state" measurements were performed, i.e., the SANS cross section was measured only for a fully (positively or negatively) polarised sample.

Another major experimental challenge was therefore the realisation of time-resolved data acquisition: due to the relatively sharp decrease of the electron-nucleus dipolar interaction, which falls off with the third power of the distance, the (close) protons in the immediate vicinity of the paramagnetic centre are polarised first, while the far away (bulk) protons equilibrate through the mechanism of spin diffusion [3]. The time constants which describe this two-step process are typically of the order of seconds. In order to resolve the initial fast polarisation build-up of the close protons, we have recently implemented time-resolved cyclic SANS data acquisition schemes [17–19], which allow the *time-dependent* SANS intensity to be measured with sufficient statistics.

Over the past few years we have undertaken a detailed study of the microscopic mechanism of DNP by means of time-resolved polarised SANS. The questions which motivated our research were the following: Is it possible at all to create locally, around a paramagnetic centre, a proton polarisation inhomogeneity which can be probed with neutron scattering techniques before it is "washed out" by spin diffusion? Can the characteristic time constants of the polarisation process be resolved? What is the size of such a proton domain, and what are the limitations of the method with respect to the concentration of radicals and the number of protons in the solvent? For our investigations on the dynamics of the nuclear polarisation process we have chosen as a model system the well-known EHBA-Cr^V complex [22]. In this molecule the Cr^V provides the unpaired electron spin and is surrounded by 20 close protons. As we will see below, although its size is only of the order of 10 Å, this length scale can be resolved with conventional SANS instruments.

In Section 2 we present details of the sample preparation and of the SANS measurements. Section 3 provides a description of the core-shell model and the approach via the integrated intensity, which were used to analyse the time dependence of the nuclear spin polarisation from time-resolved SANS data. In Section 4 we present and discuss the SANS data, and we provide a thermodynamic model in terms of rate equations, which is able to reproduce the observed concentration dependence of the time constants of the DNP process in EHBA-Cr^V. The derivation of the rate equations is detailed in the appendix.

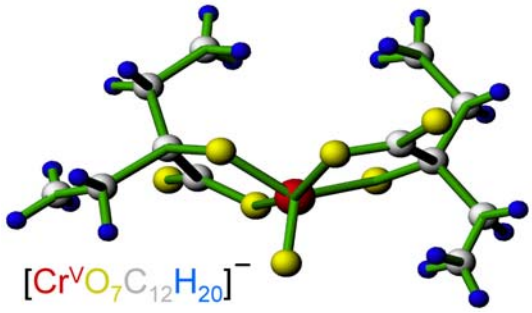

Fig. 1. The EHBA-Cr^V complex [22].

2 Experimental

A detailed report on the sample preparation, the cryostat unit, the NMR and microwave systems, and on the timing and control of DNP, NMR and neutron data acquisition can be found in reference [19]. Here, we present experimental details that are necessary in order to achieve a self-contained presentation.

2.1 Sample preparation

The samples consisted of frozen solutions of EHBA-Cr^V molecules in fully or partially deuterated glycerol-water mixtures. Figure 1 shows a sketch of the EHBA-Cr^V molecule, where the Cr^V carries the unpaired electron. Glassy slabs of dimensions $14 \times 14 \times 3$ mm were obtained by injecting the glycerol-water-EHBA-Cr^V solution into a copper mould. Best results, i.e., crack-free samples, were obtained by first pre-cooling the copper mould down to liquid nitrogen temperature, and then, depending on the relative amounts of glycerol and water (mass fraction of glycerol typically ∼55%), the solution was injected at temperatures between about 140–170 K. The subsequent sample handling was under liquid nitrogen. We have performed SANS measurements as a function of the concentration of EHBA-Cr^V, thereby probing different mean distances between the unpaired electrons, and we have varied the degree of deuteration of the glycerol-water solvent mixtures, which determines the concentration of the bulk protons. The degree of deuteration of these mixtures was chosen to be 0%, 80%, 84%, 88%, 92%, 95%, and 98%, and the concentration of EHBA-Cr^V was chosen to be $1.25 \times 10^{19}\,cm^{-3}$, $2.5 \times 10^{19}\,cm^{-3}$, and $5.0 \times 10^{19}\,cm^{-3}$.

2.2 SANS measurements

The SANS measurements were performed at the D22 instrument [25] at the Institut Laue-Langevin, Grenoble, France, at the SANS-I instrument [27] at the Paul

Scherrer Institute, Villigen, Switzerland and at PAPOL of the Laboratoire Leon Brillouin (LLB), Saclay, France. On all three instruments a time-resolved data acquisition scheme was implemented. We used polarised incident neutrons of wavelengths $\lambda = 4.6\,\text{Å}$ (ILL), $\lambda = 4.7\,\text{Å}$ (PSI), and $\lambda = 8.0\,\text{Å}$ (LLB) with a respective wavelength spread $\Delta\lambda/\lambda \cong 0.1$ (FWHM). The frozen samples were inserted into a NMR coil, placed in a microwave cavity, and mounted inside a ^{4}He-cryostat, which was operated at a temperature of about 1 K; a longitudinal static magnetic field of 3.5 T was provided by a superconducting split-coil [19]. Samples could be changed and cooled down to 1 K in less than half an hour.

Three different methods were used to establish transient polarisation gradients between the close protons and the bulk. The first two methods make use of the fact that NMR irradiation affects only the bulk protons, since those close to the paramagnetic centre have their frequency displaced[1]. A first way was to saturate the bulk protons by NMR after polarisation of the whole sample. A second way consisted in reversing the bulk polarisation with an adiabatic passage, again after polarisation of the whole sample. Both these methods have a low duty cycle since the polarising time (dead time) is long compared to the duration of the gradients (the useful measuring time). A third method — polarisation cycling — eliminated the dead time by reversing periodically the polarising frequency. This last method, besides being simple to implement, gave the most significant results.

At the ILL and PSI, two IMPATT-diodes, tuned to the frequencies required for positive and negative DNP, respectively 97.00 GHz and 97.50 GHz, could be connected to the sample cavity by a wave-guide switch (switching time ∼150 ms). At the LLB, a 70 GHz carcinotron could be switched in less than a ms between the two DNP frequencies using a line voltage step. Continuous-wave NMR was used to monitor the bulk proton polarisation. The nuclear polarisation was reversed (typically every 10 s), and the acquisition of neutron scattering intensity spectra was triggered synchronously (typically in time intervals of 0.1 s). Each of these time frames (typically 200) was averaged over several hundred cycles (typical total counting time 12 hours) to obtain sufficient statistics. The time-dependent neutron scattering $d\Sigma/d\Omega(q,t)$ was then obtained as usual by radially averaging and correction for (polarisation-dependent) transmission, background scattering, dark current, and detector efficiency. Due to the relatively small size of the EHBA-Cr^V complex (radius ∼5 Å) the sample-to-detector distance was chosen to be 1.5 m, with an additional lateral displacement of the detector of 0.45 m.

[1] Note that the dipolar interaction between the paramagnetic moments and the close protons displaces the Larmor frequency of the close nuclei far enough from the frequency of the bulk nuclei to render them "invisible" by NMR. Therefore, NMR mainly senses the bulk protons while SANS is sensitive to the close protons.

3 Core-shell model for the small-angle neutron scattering cross section of diluted EHBA-Cr^V samples

The relatively low concentrations of EHBA-Cr^V in our samples suggest that interparticle correlations in the expression for the total scattering cross section may be neglected; the average particle separation in our samples increases from roughly $c^{-1/3} \cong 30\,\text{Å}$ at a concentration of $c = 5.0\times10^{19}\,\text{cm}^{-3}$ to about 40 Å at $c = 1.25\times10^{19}\,\text{cm}^{-3}$. It may be questioned whether these crude estimates for the interparticle separation are "sufficient" to guarantee the neglect of interparticle correlations. The radially-averaged SANS data (see below) do however not show any sign of interparticle interference, so that, within the q-range studied, this assumption seems to be justified. For a set of N monodisperse non-interacting homogeneous "particles" of volume V_p embedded in a homogeneous matrix, the macroscopic differential SANS cross section $d\Sigma/d\Omega$ at scattering vector $\mathbf{q}$ can be written as [28–32]

$$\frac{d\Sigma}{d\Omega}(\mathbf{q}) = \frac{N}{V}\,\Delta\rho^2\,V_p^2\,|F(\mathbf{q})|^2 + \frac{d\Sigma_{\text{inc}}}{d\Omega}\ , \qquad (1)$$

where V is the scattering volume, $\Delta\rho^2$ denotes the squared difference between the scattering-length densities of the particle and the matrix, $F(\mathbf{q})$ is the particle form factor, and $d\Sigma_{\text{inc}}/d\Omega$ represents a generally $\mathbf{q}$-independent incoherent background term. As mentioned in the introduction, the basic idea of combining SANS and DNP originates from the spin dependence of the scattering amplitudes of nuclei possessing a non-zero nuclear spin. Since the discreteness of the atomic structure of matter cannot be resolved by small-angle scattering, the relevant quantity which contains information on the dynamics of the nuclear polarisation process is the scattering-length density ρ. The quantity ρ is defined as the sum of all the individual atomic scattering lengths of the scattering object divided by its volume. In a continuum approximation the expression for the scattering-length density (for systems with one isotope with non-zero nuclear spin) can be written in the general form

$$\rho[P(t)] = a \pm b\,P(t)\ , \qquad (2)$$

where a and b are constants, the nuclear polarisation P is a continuous variable with $-1 \le P \le 1$, and the $+(-)$ sign refers to neutron spin antiparallel (parallel) to the direction of nuclear polarisation.

In order to obtain a relatively simple closed-form expression for the particle form factor we have roughly approximated the real shape of the EHBA-Cr^V molecule as a core-shell consisting of a homogeneous nuclear spin-independent core of $[CrO_7C_4]^-$ surrounded by a homogeneous shell of $[C_2H_5]_4$, which contains the 20 protons of the molecule (compare Fig. 2). The scattering-length densities of the core and of the shell, ρ_c and ρ_s respectively, can then be calculated to be $\rho_c \cong 2.0\times10^{-6}\,\text{Å}^{-2}$ and $\rho_s(P) \cong (-1.1 \pm 15.1\,P)\times10^{-6}\,\text{Å}^{-2}$ (see, e.g., Ref. [26]).

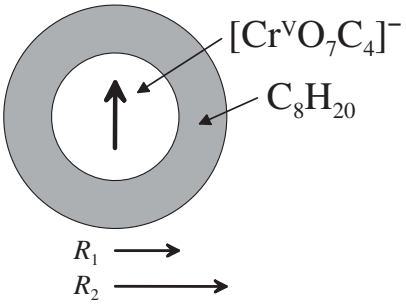

Fig. 2. Core-shell model for the EHBA-Cr^V complex. The core radius R_1 is known from crystallographic data to be about 3 Å, and $R_2 \approx 5$ Å.

The radially-averaged total SANS cross section for a set of such identical core-shells with inner radii R_1 and outer radii R_2 can then be expressed as [33]

$$\frac{d\Sigma}{d\Omega}(q) = \frac{N}{V}\left\{V_{p1}\left[\rho_c - \rho_s(P)\right]F(q,R_1) + V_{p2}\left[\rho_s(P) - \rho_m(P_b)\right]F(q,R_2)\right\}^2 + \frac{d\Sigma_{\rm inc}}{d\Omega}\ , \quad (3)$$

where $V_{p1(2)} = \frac{4\pi}{3}R_{1(2)}^3$, ρ_m is the scattering-length density of the solvent, and $F(q,R)$ denotes the scattering function of a sphere with radius R,

$$F(q,R) = 3\,\frac{\sin(qR) - qR\cos(qR)}{(qR)^3}\ . \quad (4)$$

The scattering-length density of the solvent, ρ_m, depends on the polarisation P_b of the protons in the bulk. However, at least for the fully deuterated solvents, this dependence is rather weak, so that the coherently scattered SANS intensity depends only on the polarisation of the 20 protons of the EHBA-Cr^V complex. For samples with a higher protonated solvent we have determined the bulk polarisation P_b from NMR measurements (see, e.g., Fig. 3 in Ref. [17]). The SANS data of typically 200 time frames were fitted simultaneously to equation (3) taking N/V, R_1, R_2, P, and $d\Sigma_{\rm inc}/d\Omega$ as independent parameters. In the fitting routine we have treated N/V, R_1, and R_2 as global fit parameters, constant for all curves, while P and $d\Sigma_{\rm inc}/d\Omega$ take on different values for each curve. The nuclear spin polarisation of the protons of the shell is assumed to be time dependent and spatially homogeneous, and the incoherent background was assumed to be time dependent and q-independent.

The elastic magnetic SANS cross section which is associated with the electronic magnetic moments of the EHBA-Cr^V molecules is negligible: the macroscopic differential scattering cross section $d\Sigma_p/d\Omega$ of an ensemble of randomly oriented paramagnetic spins (at zero applied magnetic field) with effective spin quantum numbers S is given by [23]

$$\frac{d\Sigma_p}{d\Omega} = \frac{N}{V}\,\frac{2}{3}\,(r_0\,\gamma)^2\,f^2\,S(S+1)\ , \quad (5)$$

where $r_0 = 2.818 \times 10^{-15}$ m is the classical radius of the electron, $\gamma = -1.913$ is the magnetic dipole moment of the neutron in units of nuclear magnetons, and f is a form factor which is close to unity in the small-angle region. For an EHBA-Cr^V concentration $N/V = 5.0 \times 10^{19}\,{\rm cm}^{-3}$, $f = 1$, and $S = 1/2$ one obtains $d\Sigma_p/d\Omega \cong 7.3 \times 10^{-6}\,{\rm cm}^{-1}\,{\rm sr}^{-1}$, which is about 4 orders of magnitude smaller than our experimental values for $d\Sigma/d\Omega$. The paramagnetic small-angle scattering increases insignificantly when the saturating magnetic field is applied perpendicular to the scattering vector (the factor 2/3 in Eq. (5) must be replaced by 1).

An alternative approach to equation (3), which allows information on the temporal evolution of the nuclear polarisation $P(t)$ to be obtained, was employed by calculating the integrated intensity Q, defined by

$$Q(t) = \int_{q_{\rm min}}^{q_{\rm max}} \left[\frac{d\Sigma}{d\Omega}(q,t) - \frac{d\Sigma_{\rm inc}}{d\Omega}(t)\right] dq\ . \quad (6)$$

For a dilute scattering system consisting of *homogeneous* monodisperse spherically-symmetric particles embedded in a *homogeneous* matrix, where the total SANS cross section can be written as the sum of single-particle scattering cross sections (compare Eq. (1)), it is readily seen that $\sqrt{Q(t)} \sim \Delta\rho(t)$, i.e., the quantity $\sqrt{Q(t)}$ is expected to reflect the time dependence of the proton polarisation of the molecules as well as of the solvent. Apart from the homogeneity of both the particles and the matrix phase, equation (6) makes no further assumptions on the microstructure of the scattering system. In other words, the two-phase approach via the integrated intensity inherently includes the time dependences of the close and of the bulk protons, and no assumption on the particular shape of the molecules is required. In contrast to the more refined analysis using the above core-shell model, equation (3), the data evaluation using equation (6), or likewise by computing the Porod invariant [34], does not provide accurate absolute values for $P(t)$.

4 Experimental results and discussion

4.1 SANS results

Different schemes have been tried to obtain initial non-equilibrium conditions. They all show clearly that a polarisation gradient between close and bulk protons can be established which lasts for a few seconds. The most significant results have been obtained by cyclic reversal of polarisation with a repetition time comparable to the characteristic polarisation times. Figure 3 shows the cyclic (time-resolved) and Figure 4 the static SANS cross sections $d\Sigma/d\Omega$ of samples with different concentrations of EHBA-Cr^V and for different degrees of solvent deuteration.

After the first few cycles needed to establish a constant dynamical regime, each cycle starts from a large negative polarisation, $-P_{\rm max}$, to end up after 10 s with

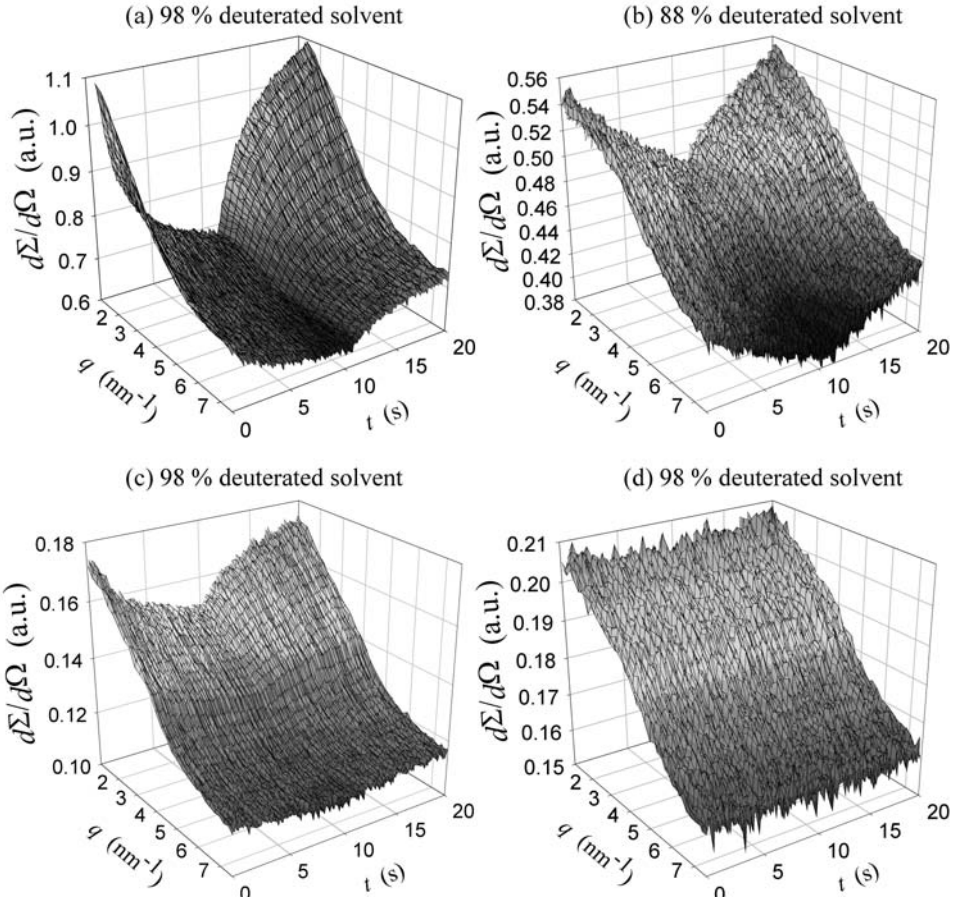

Fig. 3. Time-resolved radially-averaged SANS cross sections $d\Sigma/d\Omega$ of various EHBA-Cr^V samples as a function of the concentration c of EHBA-Cr^V and for different degrees of deuteration of the glycerol-water mixture. (a) $c = 5.0 \times 10^{19}\,\mathrm{cm}^{-3}$; (b) $c = 5.0 \times 10^{19}\,\mathrm{cm}^{-3}$; (c) $c = 2.5 \times 10^{19}\,\mathrm{cm}^{-3}$; (d) $c = 1.25 \times 10^{19}\,\mathrm{cm}^{-3}$. During the DNP cycle (positive DNP in the first 10 s and negative DNP in the next 10 s) we have typically collected 200 SANS cross sections.

a positive polarisation $+P_{\max}$. This leads to a decrease in contrast. During the following 10 s, the polarisation decreases back to $-P_{\max}$, thereby increasing the contrast (compare Figs. 3a–3c and Fig. 6). The SANS data in Figures 3 and 4a–4c can be described as consisting of a q-dependent coherent signal and of a q-independent incoherent contribution $d\Sigma_{\mathrm{inc}}/d\Omega$, in agreement with equation (3). For a given concentration c of EHBA-Cr^V and for an increasing amount of protons in the solvent the magnitude of the incoherent background term relative to the coherent part of $d\Sigma/d\Omega$ increases (compare Figs. 3a and 3b, Figs. 4a and 4b and Figs. 3c and 4c). On the other hand, leaving the solvent deuteration constant and decreasing the concentration of EHBA-Cr^V leads to a "weakening" of the time dependence of the neutron scattering signal (compare Figs. 3a, 3c and 3d). This weaker time dependence of $d\Sigma/d\Omega$ is due to a progressively larger incoherent background (relative to the coherent SANS) and is related to a decreasing dependence of the scattering contrast on the polarisation: as a consequence of the reduced concentration of EHBA-Cr^V, the associated weaker electron-electron interaction results in a less efficient DNP process. The above observations indicate the main limitations of the method: below a concentration of $c \cong 2.5 \times 10^{19}\,\mathrm{cm}^{-3}$ and for a solvent protonation higher than about 8–10% it becomes difficult to observe a coherent nuclear spin-dependent SANS signal in EHBA-Cr^V glycerol-water samples.

Substituting the 20 protons of the EHBA-Cr^V complex by deuterons and dissolving the molecules in a 98% deuterated solvent leads to a vanishing contrast for coherent SANS (compare Fig. 4d). The remaining spin dependence of the SANS cross section is predominantly due to the polarisation dependence of the incoherent scattering from the residual (2%) protons of the solvent.

Figure 5 shows the SANS intensity for a sample with 2.5×10^{19} EHBA-Cr^V complexes per cm^3 in a 98% deuterated solvent at selected times during the cyclic DNP process. The solid lines in the figure represent a fit to the core-shell model, equation (3), from which the time dependence of the close proton polarisation $P(t)$ can be deduced (see Fig. 6). Also shown in Figure 6 is $P(t)$ for a sample with the double amount of EHBA-Cr^V. A closer inspection of both curves for $P(t)$ suggests the existence of two time constants in the data: both curves show an initial fast increase of P followed by a subsequent slower

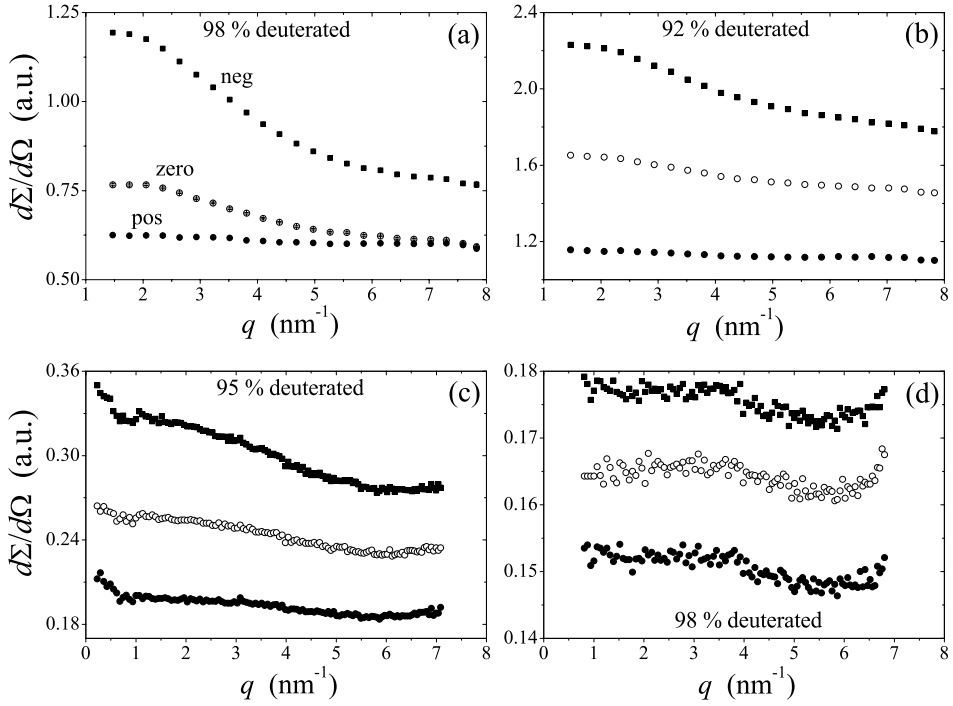

Fig. 4. Static SANS cross sections $d\Sigma/d\Omega$ of EHBA-Cr^V samples for negative, zero, and positive nuclear polarisation (from top to bottom as in (a), respectively). Concentration of EHBA-Cr^V (in $10^{19}\,cm^{-3}$). (a) 5.0; (b) 5.0; (c) 2.5. (d) Static $d\Sigma/d\Omega$ for a sample with a fully deuterated EHBA-Cr^V molecule ($c = 5.0 \times 10^{19}\,cm^{-3}$) in a 98 % deuterated solvent.

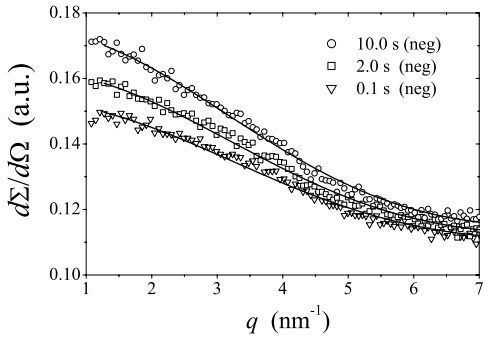

Fig. 5. $d\Sigma/d\Omega$ of EHBA-Cr^V at selected times during negative DNP (see inset). Concentration of EHBA-Cr^V is $2.5 \times 10^{19}\,cm^{-3}$, solvent is 98% deuterated. Solid lines: Global fit to the core-shell model, equation (3).

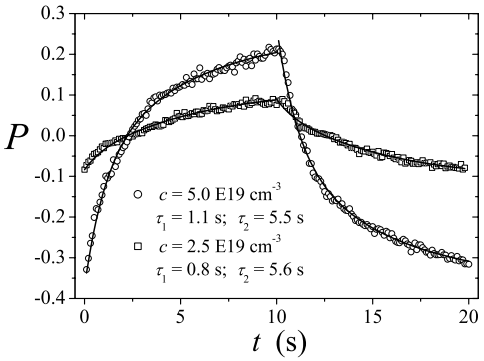

Fig. 6. Temporal evolution of the close proton polarisation $P(t)$ for different concentrations of EHBA-Cr^V (see inset) in a 98% deuterated solvent. The data points were obtained by fitting equation (3) to the time dependent SANS data shown in Figures 3a and 3c, respectively. Solid lines: Fit of the respective data set to equation (7) using the same time constants and exponential prefactors (with opposite sign) in each of the two branches.

increase. The solid lines in Figure 6 represent a fit of the respective data set to the phenomenological function

$$P(t) = A_0 + A_1 \exp(-t/\tau_1) + A_2 \exp(-t/\tau_2)\ , \qquad (7)$$

where A_0, A_1, A_2 are variable parameters. The two exponentials in equation (7) model the time dependence of the polarisations of the close and the bulk protons, where the time constants τ_1 and τ_2 are assumed to reflect respectively the faster polarisation build-up of the close protons and the slower polarisation build-up of the bulk protons. As is suggested by the results shown in Figure 7, the values of τ_1 and τ_2 are (within limits) independent of the repetition rate of the cyclic data-aquisition procedure.

The results of the (integrated intensity) analysis using equation (6) can be seen in Figure 8 for samples with 5.0×10^{19} and 2.5×10^{19} EHBA-Cr^V molecules per cm^3 in a 98% deuterated solvent. The corresponding incoherent background $d\Sigma_{inc}/d\Omega$ was estimated by averaging the measured SANS cross section $d\Sigma/d\Omega$ at the highest q-values, and a lower bound for the integrated intensity $Q(t)$ was computed according to equation (6). The solid lines in

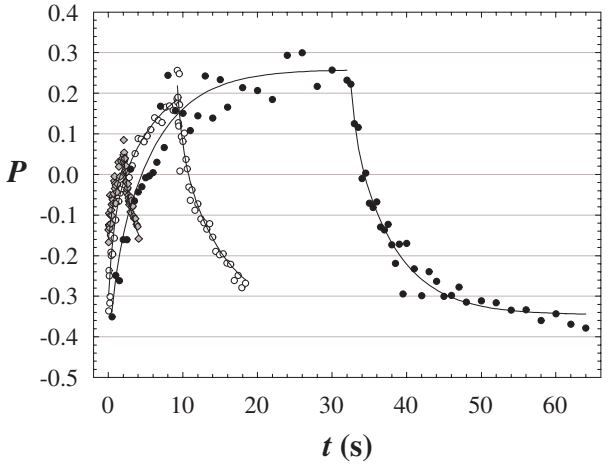

Fig. 7. Time evolution of the polarisation P for three different repetition rates in a 98 % deuterated sample [35]. The polarisations are derived from the neutron scattering by means of the core-shell model. Their time dependence is fitted to a two-reservoir model using the same time constants ($\tau_1 = 1.2\,\mathrm{s}$ and $\tau_1 = 7.0\,\mathrm{s}$). The total measuring time being constant, more short cycles have been averaged resulting in a better statistics. The two time constants agree reasonably well with those obtained on the similar samples.

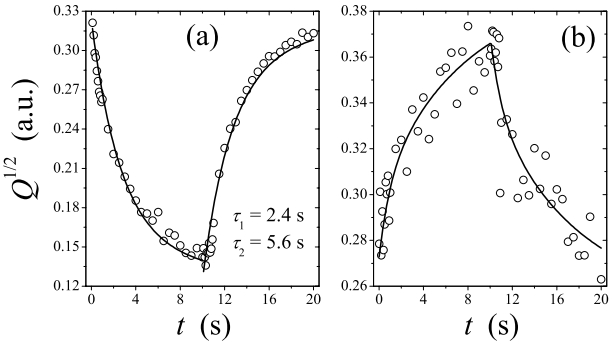

Fig. 8. (○) Time dependence of the square root of the integrated intensity $Q(t)$ for samples containing (a) 5.0×10^{19} and (b) 2.5×10^{19} EHBA-Cr^V complexes per cm^3 in 98% deuterated solvent. Solid lines: Fit to equation (7).

Figure 8 are fits of the data to equation (7), imposing the same constraints on the fit as in Figure 6. While the data in Figure 8a permits two time constants to be extracted, the large scatter in the data in Figure 8b does not allow for a reliable determination of time constants. The values of the time constants, $\tau_1 \cong 2.4\,\mathrm{s}$ and $\tau_2 \cong 5.6\,\mathrm{s}$, are in reasonable agreement with the corresponding values obtained from the core-shell model (see Fig. 10 below), thereby providing *independent* support for the appropriateness of the core-shell model.

Another independent check of the reality of the polarisation inhomogeneity between close and bulk protons is shown in Figure 9. It shows the time evolution of the incoherent scattering with respect to the coherent scattering. The former depends to a large part on the polarisation of

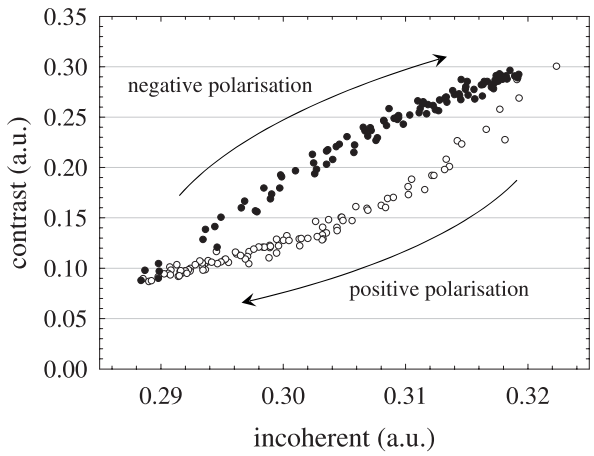

Fig. 9. Scattering contrast vs. incoherent scattering during cyclic polarisation in a sample with 98% deuterated solvent [35].

the bulk protons, even in our deuterated solvents, while the latter is predominantly dependent on the contrast of the EHBA-Cr^V molecule, i.e., the polarisation of the close protons. The hysteresis over a full polarisation cycle is a clear sign of a time-dependent polarisation inhomogeneity in each half-cycle.

Figure 10 depicts the results for the time constants (obtained from the core-shell model) as a function of the number of protons in the solvent. For the samples studied, τ_1 decreases with increasing number of protons in the solvent, while τ_2 follows the opposite trend. As we will see in the next section, a thermodynamic model, based on rate equations expressing the flow of polarisation between three thermal reservoirs, is able to reproduce the observed dependence of τ_1 and τ_2 on the concentration of protons in the solvent.

4.2 Thermodynamic "one-centre" model for the dynamics of the nuclear polarisation process

The temporal evolution of the close proton polarisation $P(t)$ (Fig. 6) can be described as a sum of a constant and two exponentials with time constants τ_1 and τ_2, according to equation (7). This behaviour suggests an interpretation in terms of rate equations describing the flow of polarisation between three thermal reservoirs coupled in series. The reservoirs can be identified as follows: the electronic spin-spin interaction reservoir R_0, which is cooled by the microwaves and acts as a "source" of polarisation; a reservoir R_1 constituted by the 20 protons of the complex and coupled to this source; a reservoir R_2 formed by the bulk protons and coupled to R_1. See Figure 11 for a sketch of the reservoir model.

Two rate equations govern the dynamics:

$$\frac{dP_1}{dt} = \frac{W_{01}}{N_1}(P_0 - P_1) + \frac{W_{12}}{N_1}(P_2 - P_1) \qquad (8)$$

$$\frac{dP_2}{dt} = \frac{W_{12}}{N_2}(P_1 - P_2)\ .$$

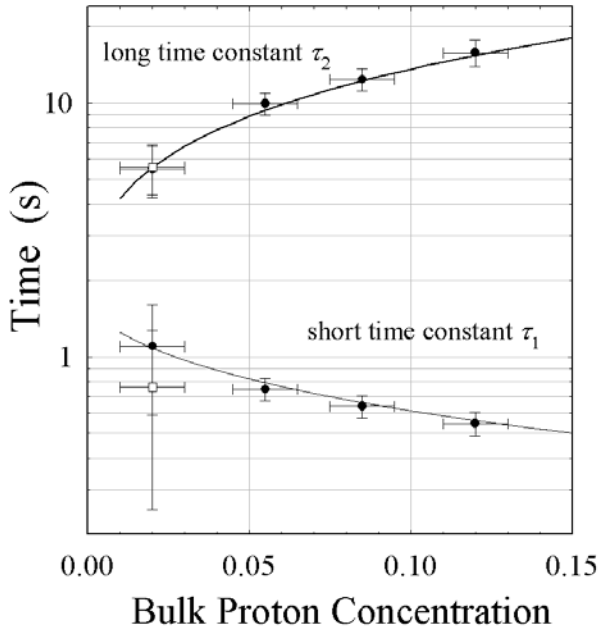

Fig. 10. Dependence of the time constants τ_1 and τ_2 (determined from the analysis of the corresponding $P(t)$ curves) on the proton concentration of the solvent. (•) $c = 5.0\times10^{19}$ cm^{-3}; (□) $c = 2.5\times10^{19}$ cm^{-3}. Solid lines: Solutions of the rate equations (8). Data partly taken from reference [19].

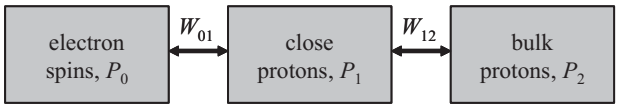

Fig. 11. The one-centre reservoir model illustrating the flow of polarisation between the electron-spin reservoir R_0, the close-proton reservoir R_1, and the reservoir R_2 which is formed by the solvent protons. W_{01} and W_{12} are coupling constants.

N_i and P_i $(i = 1, 2)$ denote the number and polarisation of protons belonging to the reservoir R_i, and $P_0 \cong 1$ denotes the polarisation of the source. The rate constants W_{ij} are defined as probabilities of a mutual spin flip per time unit. W_{01} characterises the flow of polarisation from R_0 to R_1, and W_{12} characterises the coupling of the reservoirs R_1 and R_2. The general solution of the above set of coupled first-order differential equations (8) is derived in the appendix. The two time constants τ_1 and τ_2 depend only on the ratios N_1/N_2 and W_{01}/W_{12}. For the sample with 98 % deuteration of the solvent and $c = 5.0 \times 10^{19}$ cm^{-3}, the unknown values of W_{01} and W_{12} are adapted so that the values of τ_1 and τ_2, which are determined from the analysis of $P(t)$ (Fig. 6), coincide with the time constants of the model solutions of equations (8). In order to extrapolate these time constants to higher bulk proton concentration c_b we assume W_{01} as concentration-independent, and we make the Ansatz $W_{12} \sim c_b^{\beta}$. The best agreement with the experimental time constants is found for $\beta = 0.8$. The solid lines in Figure 10 represent the prediction of the one-centre reservoir model for the bulk proton concentration dependence of the time constants τ_1 and τ_2. The long time constant τ_2 essentially describes the build-up of the bulk proton polarisation. It is slowed down with increasing bulk proton concentration due to the heat capacity of R_2 being proportional to c_b. The dependence of the short time constant τ_1 on c_b can be partly understood as being due to a "loading" effect of R_2 on R_1 induced by a better coupling between these reservoirs.

5 Summary and conclusions

We have provided an analysis of the nuclear spin-dependent small-angle neutron scattering (SANS) from domains of polarised protons in deuterated glycerol-water solutions of EHBA-Cr$^{\mathrm{V}}$ molecules. By means of dynamic nuclear polarisation we have locally created a nuclear polarisation contrast around the Cr$^{\mathrm{V}}$ paramagnetic centres. We have varied the concentration of EHBA-Cr$^{\mathrm{V}}$ and the number of protons of the solvent. Below a concentration of EHBA-Cr$^{\mathrm{V}}$ molecules of roughly 2.5×10^{19} cm^{-3} (in a fully deuterated solvent) we did not observe any appreciable time dependence of the SANS curves. Likewise, for a proton concentration of the solvent larger than about 8–10% the increased magnitude of the incoherent scattering did not allow a coherent SANS signal to be observed. The radially-averaged SANS curves could be analysed successfully using a model of non-interfering core-shells. The simultaneous global fitting of typically 200 time-resolved $d\Sigma/d\Omega$ data sets provided the time dependence $P(t)$ of the close proton polarisation. Two time constants, τ_1 and τ_2, could be identified in the dynamics of the polarisation process. The short time constant τ_1, typically of the order of 1 s, can be related to the relatively fast polarisation build-up of the protons close to the paramagnetic centre, whereas the long-time constant τ_2 (∼10 s) was interpreted as describing the slower polarisation build-up of the polarisation of the distant bulk protons of the solvent. A thermodynamic model expressing the flow of polarisation between three reservoirs coupled in series is able to reproduce the concentration dependence of the experimental time constants.

Appendix

Equations (8) describing the flow of polarisation between the three reservoirs can be written in dimensionless form as

$$\frac{dP_1}{d\tau} = w\,(P_0 - P_1) + (P_2 - P_1)$$
$$\frac{dP_2}{d\tau} = n\,(P_1 - P_2)\ ,$$

where $w = W_{01}/W_{12}$, $n = N_1/N_2$, and $\tau = (W_{12}/N_1)\,t$. The general solution is

$$P_1(\tau) = A\,\exp(-g_1\,\tau) + B\,\exp(-g_2\,\tau) + P_0$$
$$P_2(\tau) = C\,\exp(-g_1\,\tau) + D\,\exp(-g_2\,\tau) + P_0\ .$$

The two rate constants $g_{1,2} = 1/2\,[(1+w+n) \pm r]$ with $r = [(1+w+n)^2 - 4\,w\,n]^{1/2}$ are independent of the boundary conditions. Identification with the observed time constants τ_1 and τ_2 gives $\tau_i = N_1/(W_{12}\,g_i)$ with $i = 1, 2$. The amplitudes are

$$A = \frac{C\,(n - g_1)}{n}\ ,$$
$$B = \frac{D\,(n - g_2)}{n}\ ,$$
$$C = \frac{(g_2 - n)\,\Delta P_2 + n\,\Delta P_1}{g_2 - g_1}\ ,$$
$$D = \frac{(g_1 - n)\,\Delta P_2 + n\,\Delta P_1}{g_1 - g_2}\ ,$$

where $\Delta P_i = P_i - P_0$ with $i = 1{,}2$. For alternating polarisations with long cycling times, one has the initial conditions $P_1(\tau = 0) = P_2(\tau = 0)$. The largest polarisation difference during each half cycle is then easily calculated as

$$\Delta P_{\max} = \frac{|P_2 - P_1|_{\max}}{P_0} = \frac{w}{r}\,[\exp(-g_1\,\tau_{\max}) - \exp(-g_2\,\tau_{\max})]\ ,$$

which is reached after a time $\tau_{\max} = \ln(g_2/g_1)/(g_2 - g_1)$. According to this model, it is not possible to obtain large polarisation gradients for $w \ll 1$, i.e., for slow polarisation compared to spin-diffusion if one uses the method of polarisation cycling. In these cases, the more favorable initial conditions achievable with periodic saturation or adiabatic reversal may largely compensate for the lower duty cycles.

References

1. A. Abragam, *The Principles of Nuclear Magnetism* (Oxford University Press, Oxford, 1961), Chap. 9
2. A. Abragam, M. Goldman, Rep. Prog. Phys. **41**, 395 (1978)
3. A. Abragam, M. Goldman, *Nuclear Magnetism, Order and Disorder* (Oxford University Press, Oxford, 1961), Chap. 6
4. H. Glättli, M. Goldman, in *Methods of Experimental Physics* (Academic Press, New York, 1987), Vol. 23, part C, pp. 241-286
5. V.I. Lushchikov, Yu.V. Taran, F.L. Shapiro, Soviet J. Nucl. Phys. **10**, 669 (1970)
6. A. Abragam, G.L. Bacchella, C. Long, P. Meriel, J. Peisvaux, M. Pinot, Phys. Rev. Lett. **28**, 805 (1972)
7. J.B. Hayter, G.T. Jenkin, J.W. White, Phys. Rev. Lett. **33**, 696 (1974)
8. M. Leslie, G.T. Jenkin, J.B. Hayter, J.W. White, S. Cox, G. Warner, Phil. Trans. R. Soc. Lond. B **290**, 497 (1980)
9. K. Motoya, M. Nishi, Y. Ito, Solid State Comunn. **33**, 143 (1980)
10. W. Knop, K. H. Nierhaus, V. Novotny, T.O. Niinikoski, M. Krumpolc, J.M. Rieubland, A. Rijllart, O. Schärpf, H.-J. Schink, H.B. Stuhrmann, R. Wagner, Helv. Phys. Acta. **59**, 741 (1986)
11. M. Kohgi, M. Ishida, Y. Ishikawa, S. Ishimoto, Y. Kanno, A. Masaike, Y. Masuda, K. Morimoto, J. Phys. Soc. Jpn. **56**, 2681 (1987)
12. W. Knop, H.-J. Schink, H.B. Stuhrmann, R. Wagner, M. Wenkow-Es-Souni, O. Schärpf, M. Krumpolc, T.O. Niinikoski, M. Rieubland, A. Rijllart, J. Appl. Cryst. **22**, 352 (1989)
13. H. Glättli, C. Fermon, M. Eisenkremer, J. Phys. **50**, 2375 (1989)
14. M.G.D. van der Grinten, H. Glättli, M. Pinot, Neutron News **6**, 18 (1995)
15. R. Willumeit, N. Burkhardt, G. Diedrich, J. Zhao, K.H. Nierhaus, H.B. Stuhrmann, J. Mol. Struct. **383**, 201 (1996)
16. H.B. Stuhrmann, B. van den Brandt, P. Hautle, J.A. Konter, T.O. Niinikoski, M. Schmitt, R. Willumeit, J. Zhao, S. Mango, J. Appl. Cryst. **30**, 839 (1997)
17. B. van den Brandt, H. Glättli, I. Grillo, P. Hautle, H. Jouve, J. Kohlbrecher, J.A. Konter, E. Leymarie, S. Mango, R.P. May, H.B. Stuhrmann, O. Zimmer, Europhys. Lett. **59**, 62 (2002)
18. B. van den Brandt, H. Glättli, I. Grillo, P. Hautle, H. Jouve, J. Kohlbrecher, J.A. Konter, E. Leymarie, S. Mango, R.P. May, H.B. Stuhrmann, O. Zimmer, Physica B **335**, 193 (2003)
19. B. van den Brandt, H. Glättli, I. Grillo, P. Hautle, H. Jouve, J. Kohlbrecher, J.A. Konter, E. Leymarie, S. Mango, R. May, A. Michels, H.B. Stuhrmann, O. Zimmer, Nucl. Instr. and Meth. A **526**, 81 (2004)
20. H.B. Stuhrmann, Rep. Prog. Phys. **67**, 1073 (2004)
21. C.G. Shull, R.P. Ferrier, Phys. Rev. Lett. **10**, 295 (1963)
22. M. Krumpolc, J. Roček, J. Am. Chem. Soc. **101**, 3206 (1979)
23. G.E. Bacon, *Neutron Diffraction* (Clarendon Press, Oxford, 1955), Chap. 6
24. R.M. Moon, T. Riste, W.C. Koehler, Phys. Rev. **181**, 920 (1969)
25. See `http://www.ill.fr/YellowBook/D22/`
26. See `http://www.ncnr.nist.gov/resources/sldcalc.html`
27. J. Kohlbrecher, W. Wagner, J. Appl. Cryst. **33**, 804 (2000)
28. A. Guinier, G. Fournet, *Small-Angle Scattering of X-Rays* (Wiley, New York, 1955)
29. *Small-Angle X-ray Scattering*, edited by O. Glatter, O. Kratky (Academic Press, London, 1982)
30. S.-H. Chen, T.-L. Lin, in *Neutron Scattering*, edited by K. Sköld, D. L. Price (Academic Press, San Diego, 1987), vol. 23–Part B, pp. 489–543.
31. L.A. Feigin, D.I. Svergun, *Structure Analysis by Small-Angle X-Ray and Neutron Scattering* (Plenum, New York, 1987)
32. P. Lindner, T. Zemb, *Neutron, X-Ray and Light Scattering: Introduction to an Investigative Tool for Colloidal and Polymeric Systems* (North Holland, Amsterdam, 1991)
33. I. Marković, R.H. Ottewill, Colloid Polymer Sci. **264**, 65 (1986)
34. G. Porod, Kolloid-Z. **124**, 83 (1951)
35. E. Leymarie, *Méthodes de variation de contraste par polarisation nucléaire en diffusion de neutrons aux petits angles*, Thèse de Doctorat de l'Université Paris XI (N° D'ordre: 7052), (`http://tel.ccsd.cnrs.fr/documents/archives0/00/00/21/03`), unpublished (2002)